Comparison of the Optimal Design of Spinal Hybrid Elastic Rod for Dynamic Stabilization: A Finite Element Analysis

Jui-Yang Hsieh
Department of Biomedical Engineering, National Taiwan University
Chen-Sheng Chen
Department of Physical Therapy and Assistive Technology, National Yang Ming Chiao Tung University
Jyh-Horng Wang
Department of Biomedical Engineering, National Taiwan University
Po-Quang Chen
Department of Biomedical Engineering, National Taiwan University
Yi-You Huang (j00237703559@gmail.com)
Department of Biomedical Engineering, National Taiwan University

Research Article

Keywords: spine hybrid elastic rod, finite element analysis, poly (carbonate urethane), nitinol, dynamic stabilization

Posted Date: April 12th, 2022

DOI: https://doi.org/10.21203/rs.3.rs-1508018/v1

Abstract

Introduction: Dynamic stabilization can fix deformities, fractures, and disc degeneration of the spine. Nitinol and poly(carbonate urethane) (PCU) are applicable elastic biomedical materials. The spinal hybrid elastic (SHE) rod is a semirigid pedicle screw-based rod intended for use with universal pedicle screws. This study aimed to investigate the biomechanical effects of different ratios of SHE rod using finite element analysis (FEA).

Methods: A 3-dimensional nonlinear FEA of an intact lumbar spine model (INT) was constructed. The system was composed of pedicle screws, an inner nitinol stick (NS), and an outer PCU shell (PS). Four groups of models were constructed with the same outer diameter (5.5 mm) as the SHE rod. These groups had different NS diameter/PS thickness ratios: Nt45 (4.5/1.0), Nt35 (3.5/2.0), Nt25 (2.5/3.0), and Nt15 (1.5/4.0). After implanting at L3-L4, they were compared with INT. The resultant intervertebral range of motion (ROM), disc stress, facet joint contact force, screw stress, NS stress, and PCU stress were analyzed.

Results: The overall trend in results indicated that ROM, disc stress, and facet force decreased moderately in the implanted L3-L4 levels, and increased slightly in the adjacent L2-L3 levels. NS stress and the NS diameter trended towards inverse proportionality. Changing the ratio did not markedly influence screw or PS stress.

Conclusions: The SHE rod system provided sufficient spinal support and increased gentle adjacent-segment stress. The optimal NS diameter/PS thickness ratio of the SHE rod system is 4.5/1.0 mm or 3.5/2.0 mm due to the lower stress concentrations for the durability of the implant.

Background

Posterior spinal instrumentation with the pedicle screw-based system is indicated for the treatment of scoliosis, kyphosis, vertebral fractures, spondylolisthesis, spondylolysis, and degenerative disc diseases [1, 2]. Fusion with interbody fusion can more effectively strengthen spinal fixation [3, 4]. However, various complications are associated with poor fixation and ineffective fusion [5]. Rigid fusion not only fixes the surgical spine, but also increases the displacement and pressure of adjacent levels, and can thus result in adjacent segment disease (ASD) and failed back surgery syndrome (FBSS) [6, 7].

A nonfusion dynamic stabilization system has previously been developed to support the spine and preserve physiological functions. This system reduces the risks of ASD and FBSS [8, 9]; however, existing systems have shortcomings such as complex structures, difficult operation, and lack of durability [10, 11]. To design a perfect dynamic stabilization system, the mechanical structure and material selection should be simultaneously improved [12, 13].

The spinal hybrid elastic (SHE) rod is a semirigid pedicle screw-based rod intended for use with universal pedicle screws. The SHE rod was composed of an inner nitinol stick (NS) and an outer poly(carbonate

urethane) (PCU) shell (PS). This finite element analysis (FEA) analysis study was conducted to investigate the precise ratio of the thicknesses of the NS and PS. We hypothesized that an optimal SHE rod can provide sufficient spine support, gentle adjacent segment stress, and remarkable durability.

Materials And Methods

Finite element model construction of the lumbar spine

A three-dimensional, nonlinear finite element model of the human lumbar spine was created using the commercial software ANSYS 14.5 (ANSYS Inc., Canonsburg, PA, USA). The material properties of the intact lumbar spine model (INT) have been investigated in previous studies (Table 1) [14–17]. The range of motion (ROM) of the INT was compared with that of cadaveric specimens in in vitro testing. The reliability and similar stiffness were validated [18]. The present mesh density was selected based on the convergence test and the model validated in our previous studies [14, 16]. Overall, the discrepancy between the in vitro tests and our finite element simulation was within one standard deviation. The model also contained intervertebral discs, endplates, posterior bony elements, and seven ligaments. These intervertebral discs were composed of a ground substance, hyperelastic annulus fibrosus, and incompressible nucleus pulposus with 12 double-cross-linked fiber layers embedded in the ground substance.

Boundary And Loading Conditions

All models were constrained at the bottom of the L5 vertebrate. For INT, two load steps were imposed within the finite element models. During the first loading step, a perpendicular axial force of 150 N was loaded to the top of the L1 spine. In the second load step, a pure unconstrained moment was applied to ensure that the resultant ROM of the L1 to L5 spine was equal for all motions. The displacement control angle was determined using the minimally incremental force method. Applying a constant ROM has been proven to be applicable in predicting adjacent segment effects after spinal implantation [16]. The resultant intervertebral ROM and stress of the intervertebral disc and facet joint contact forces were analyzed. Distortion energy theory was applied to the intervertebral discs. The von Mises stress of each model was obtained after applying torque in each direction of the model.

Fea Construction Of Implants

Four pedicle screws and two SHE rods were implanted at the L3-L4 level of the spinal model. The material parameters of each element were obtained from previous research [17, 19] (Table 2). The diameter of the titanium alloy pedicle screw was set to 6.4 mm without threads. The interface between the pedicle screw, bone, PS, and NS was simulated for the bonded contact. The SHE rod is composed of an inner NS and outer PS. The outer diameter of the SHE rod was uniformly set to 5.5 mm. These groups had different NS diameter/PS thickness ratios: Nt45 (4.5/1.0), Nt35 (3.5/2.0), Nt25 (2.5/3.0), and Nt15 (1.5/4.0). (Fig. 1).

Results

This paper presents the results in two parts. First, the ROM, disc stress, and facet force in the instrumented groups were compared to those in the INT group. Second, the biomechanical behavior of the screw, NS, and PS was compared to that of Nt45.

The intervertebral ROM

At the implanted L3-L4 levels, the ROM in all models decreased compared with the INT, do a degree of 56-62% in extension, which is similar to flexion (57-60%). The ROM further decreased by 4-18% in torsion and 49-57% in lateral bending. In contrast, the ROM of the cephalic adjacent L2-L3 levels all increased; by 17-19% during flexion, 13-15% during extension, 1-5% during torsion and 14-17% during lateral bending (Table 3).

Overall, the differences between these models were within 5% for both flexion and extension. There was a downward trend in ROM changes at all levels as the NS diameter decreased (Figure 2).

Intervertebral disc stress

At the implanted L3-L4 level, the disc stress in all models decreased when compared with INT (Table 4). The disc stress decreased by 31-33% in flexion, where the maximum occurred in the anterior superior edge; 42-43% in extension, where the maximum occurred in the posterior inferior edge; 3-19% in torsion, where the maximum occurred in the left inferior edge; and by 45-55% in lateral bending, where the maximum occurred in the left superior edge.

In contrast, the disc stress of the cephalic L2-L3 adjacent levels all increased. This parameter increased by 24-27% in flexion, where the maximum occurred in the anterior superior edge (Figure 3); by 12-14% in extension, where the maximum occurred in the posterior inferior edge; by 0-7% in torsion, where the maximum occurred in the left inferior edge; and by 21-24% in lateral bending, where the maximum occurred in the left superior edge.

Overall, the differences between these models were within 10%, except for torsion at the implant level. The NS diameter was inversely proportional to the disc stress at the implant level. It did not markedly influence the disc stress at the adjacent level (Figure 4).

Facet joint contact force

There was no facet force during flexion in any of the models. At the implanted L3-L4 levels, the facet force in all models decreased compared with the INT, by 87-95% in extension, 4-37% in torsion and 79-100% in lateral bending. The Nt45 model showed the greatest decrease (Table 5).

In contrast, the facet force of the adjacent cephalic L2-L3 levels all increased, by 23-25% and 40-55% in extension and lateral bending, respectively, where the maximum occurred on Nt35, while it increased by 2-11% in torsion, and the maximum occurred on Nt45.

Screw stress

In flexion, the screw stress on Nt35 increased by 1% when compared with Nt45, whereas the other models decreased by 4-6%. The screw stress increased by 5-7% and 11-15% during extension and lateral bending, respectively, and decreased by 23-53% in torsion. For all motions, the screw stress of all models ranged between 98.9 and 211 MPa, and the maximum occurred on Nt45 in torsion (Table 6).

PS stress

In flexion and lateral bending, the PS stress increased by 4% and 6% on Nt15 compared to Nt45. Except for these two models, the other models decreased by 26-74%. There was no obvious trend in PS stress as the NS diameter changed (Figure 5). In all motions, the PS stress of all the models was between 2.7 and 17.4 MPa, and the maximum occurred on the Nt45 in torsion (Table 6).

NS stress

In flexion, extension, torsion, and lateral bending, the NS stress increased by 24-168%, 16-156%, 48-75% and 14-117% when compared with Nt45 (Table 6). The NS stress increased as the NS diameter decreased, and the maximum stress occurred in the lower-third portion (Figure 6). For all motions, the NS stress of all models was between 39.5 and 383 MPa, and the maximum occurred on Nt25 in torsion (Figure 7).

SHE rod stress

The SHE rod stress comprises both the PS and NS stresses. In flexion, extension, torsion, and lateral bending, the SHE rod stress increased by 18-152%, 9-137%, 40-65% and 12-111% when compared with Nt45, and the greatest increase occurred on Nt15. The SHE rod stress increases as the NS diameter decreases. For all motions, the SHE rod stress of all models was between 44.6 and 389 MPa, and the maximum occurred on Nt25 in torsion.

Discussion

The SHE rod dynamic stabilization system is intended to balance the stability and motion of the spine after surgery. In this study, the overall trend indicated that ROM, disc stress, and facet force decreased moderately in the implanted L3-L4 levels, and increased mildly in the adjacent L2-L3 levels. Nevertheless, the stress shielding effect on adjacent levels is still less than that of a rigid fixator [20]. The fusion FEA showed more extreme biomechanical changes at the surgical and adjacent levels [14]. The present results demonstrate that the SHE rod can provide good spinal stability and avoid high loading at the adjacent levels.

No single clinical material can exhibit biphasic rigidity and flexibility. Therefore, we propose the hybrid use of semi-rigid and flexible materials. The semi-rigid nitinol is used for the inner stick, and the flexible

PCU is used for the outer shell. A commercially available SHE rod was devised based on the results of the precise ratio of the hybrid used in this study.

Nitinol is an elastic shape-memory alloy that minimizes stress shielding, which has even been shown to trend toward superior fatigue resistance compared with titanium [21]. However, nitinol is not a popular material in orthopaedic applications because of its poor corrosion resistance and anti-wear properties [22]. To this end, we introduced a PCU polymer as an insulator. The outer PCU shell enveloped the inner Nitinol stick, providing perfect insulation against the titanium screw heads and nuts. In the present FEA, the NS stress increased markedly in the upper and lower portions. This phenomenon is directly related to the connection between the screw head and nut. Nevertheless, the NS stress was always lower than the yield strength of nitinol (816MPa) [23]. NS in the SHE system has a low potential implant failure rate.

The spacer in the Dynesys system is made of PCU, which is the same material as PS [18]. The stabilization of the pretension provided by the spacer and cord in Dynesys differs from that in the SHE rod system. In addition, PCU is less rigid than nitinol. The outer PS stress decreased under the same load owing to the stress shielding by the inner NS. As such, we observed no obvious trend in PS stress as the NS diameter was changed. In most of the present models, the PS stress decreased. The maximum PS stress was still much lower than the mean tensile strength of the PCU (30MPa) [13]. In addition to the materials, the structure and ratio of the hybrid in Dynesys were different from those in the SHE rod system. Therefore, the Dynesys system did not demonstrate exactly similar results to the present study [24, 25].

This study had some limitations. All spinal models were healthy with no pathological properties or defects. Degeneration or fractures are common in patients, and posterior decompression is often performed following spinal fixation. As such, the models we applied did not exactly coincide with common clinical situations. The interface between the pedicle screw and PS was simulated to be bonded, as was that between the PS and NS. The model presents an idealized fabrication of the SHE rod.

In conclusion, the SHE rod system provides sufficient spinal support and increases gentle adjacent segment stress. The optimal NS diameter/PS thickness ratio of the SHE rod system is 4.5/1.0 mm or 3.5/2.0 mm due to the lower stress concentrations for the durability of the implant.

Abbreviations

PCU: poly(carbonate urethane)

SHE: spinal hybrid elastic

FEA: finite element 31 analysis

INT: intact lumbar spine model

NS: inner nitinol stick

PS: outer PCU shell

ROM: range of 37 motion

ASD: adjacent segment disease

FBSS: failed back surgery syndrome

Declarations

Consent for publication.

Not applicable. Our study does not require consent for publication from participants.

Ethics approval and consent to participate

Not applicable. Our manuscript does not report on or involve the use of any animal or human data or tissue.

Availability of data and materials

The raw data and materials used and analysed during the current study are in a supplementary file. The further detailed datasets are available from the author JYH on reasonable request.

Competing interests

The authors declare that they have no competing interests.

Funding

The authors, their immediate families, and any research foundations with which they are affiliated have not received any financial payments or other benefits from any commercial entity related to the subject of this article.

Authors' contributions

JYH participated in the conception and design of the study, acquisition of the data, analysis and interpretation of the data, drafting, and final preparation of the manuscript. YYH participated in the conception and design of the study, acquisition of the data, analysis and interpretation of the data, drafting, and final preparation of the manuscript. CSC participated in the conception and design of the study, acquisition of the data, analysis and interpretation of the data, and final preparation of the manuscript. JHW and PQC participated in the conception and design of the study, acquisition of the data, analysis and interpretation of the data, and final preparation of the manuscript. All authors read and approved the final manuscript. Conception and design of the study, data analysis and interpretation, and manuscript writing.

Acknowledgements

This study was approved by National Taiwan University Hospital and its Jinshan branch. The authors wish to thank all the members who participated in this study.

Authors' information

Affiliations.

Department of Biomedical Engineering National Taiwan University, Taipei, Taiwan (R.O.C.)

Jui-Yang Hsieh & Yi-You Huang.

Department of Physical Therapy and Assistive Technology, National Yang Ming Chiao Tung University, Taipei, Taiwan, Taiwan (R.O.C)

Chen-Sheng Chen.

Department of Orthopedic Surgery National Taiwan University Hospital, Taipei, Taiwan (R.O.C.)

Jui-Yang Hsieh, Jyh-Horng Wang & Po-Quang Chen.

Department of Orthopedic Surgery National Taiwan University Hospital Jinshan branch, Taipei, Taiwan (R.O.C.)

Jui-Yang Hsieh.

References

1. Lykissas MG, Jain VV, Nathan ST, Pawar V, Eismann EA, Sturm PF, Crawford AH. Mid- to long-term outcomes in adolescent idiopathic scoliosis after instrumented posterior spinal fusion: a meta-analysis. Spine. 2013;38(2):E113-119.
2. Noorian S, Sorensen K, Cho W. A systematic review of clinical outcomes in surgical treatment of adult isthmic spondylolisthesis. Spine J. 2018;18(8):1441–1454.
3. Mobbs RJ, Phan K, Malham G, Seex K, Rao PJ. Lumbar interbody fusion: techniques, indications and comparison of interbody fusion options including PLIF, TLIF, MI-TLIF, OLIF/ATP, LLIF and ALIF. J Spine Surg. 2015;1(1):2–18.
4. Levin JM, Tanenbaum JE, Steinmetz MP, Mroz TE, Overley SC. Posterolateral fusion (PLF) versus transforaminal lumbar interbody fusion (TLIF) for spondylolisthesis: a systematic review and meta-analysis. Spine J. 2018;18(6):1088–1098.
5. Hu YH, Niu CC, Hsieh MK, Tsai TT, Chen WJ, Lai PL. Cage positioning as a risk factor for posterior cage migration following transforaminal lumbar interbody fusion - an analysis of 953 cases. BMC Musculoskelet Disord. 2019;20(1):260.

6. Zhang C, Berven SH, Fortin M, Weber MH. Adjacent Segment Degeneration Versus Disease After Lumbar Spine Fusion for Degenerative Pathology: A Systematic Review With Meta-Analysis of the Literature. Clin Spine Surg. 2016;29(1):21–29.
7. Sebaaly A, Lahoud MJ, Rizkallah M, Kreichati G, Kharrat K. Etiology, Evaluation, and Treatment of Failed Back Surgery Syndrome. Asian Spine J. 2018;12(3):574–585.
8. Pan A, Hai Y, Yang J, Zhou L, Chen X, Guo H. Adjacent segment degeneration after lumbar spinal fusion compared with motion-preservation procedures: a meta-analysis. Eur Spine J. 2016;25(5):1522–1532.
9. Lee CH, Jahng TA, Hyun SJ, Kim CH, Park SB, Kim KJ, Chung CK, Kim HJ, Lee SE. Dynamic stabilization using the Dynesys system versus posterior lumbar interbody fusion for the treatment of degenerative lumbar spinal disease: a clinical and radiological outcomes-based meta-analysis. Neurosurg Focus. 2016;40(1):E7.
10. Wu AM, Zhou Y, Li QL, Wu XL, Jin YL, Luo P, Chi YL, Wang XY. Interspinous spacer versus traditional decompressive surgery for lumbar spinal stenosis: a systematic review and meta-analysis. PLoS One. 2014;9(5):e97142.
11. Phan K, Rao PJ, Ball JR, Mobbs RJ. Interspinous process spacers versus traditional decompression for lumbar spinal stenosis: systematic review and meta-analysis. J Spine Surg. 2016;2(1):31–40.
12. Kok D, Firkins PJ, Wapstra FH, Veldhuizen AG. A new lumbar posterior fixation system, the memory metal spinal system: an in-vitro mechanical evaluation. BMC Musculoskelet Disord. 2013;14:269.
13. Kojio K, Furukawa M, Motokucho S, Shimada M, Sakai M. Structure-mechanical property relationships for polycarbonate urethane elastomers with novel soft segments. Macromolecules. 2009;42(21):8322–8327.
14. Chen SH, Zhong ZC, Chen CS, Chen WJ, Hung C. Biomechanical comparison between lumbar disc arthroplasty and fusion. Med Eng Phys 2009;31(2):244–53.
15. Liu CL, Zhong ZC, Shih SL, Hung CH, Lee YE, Chen CS. Influence of Dynesys system screw profile on adjacent segment and screw. J Spinal Disord Tech. 2010;23(6):410–417.
16. Zhong ZC, Chen SH, Hung CH. Load- and displacement-controlled finite element analyses on fusion and non-fusion spinal implants. Proc Inst Mech Eng H. 2009;223(2):143–157.
17. Liu CL, Zhong ZC, Hsu HW, Shih SL, Wang ST, Hung C, Chen CS. Effect of the cord pretension of the Dynesys dynamic stabilization system on the biomechanics of the lumbar spine: a finite element analysis. Eur Spine J. 2011;20(11):1850–1858.
18. Yamamoto I, Panjabi MM, Crisco T, Oxland T. Three-dimensional movement of the whole lumbar spine and lumbosacral joint. Spine. 1989;14:1256–1260.
19. Chevalier V, Arbab-Chirani R, Arbab-Chirani S, Calloch S. An improved model of 3-dimensional finite element analysis of mechanical behavior of endodontic instruments. Oral Surg Oral Med Oral Pathol Oral Radiol Endod. 2010;109(3):111–21.
20. Rohlmann A, Burra NK, Zander T, Bergmann G. Comparison of the effects of bilateral posterior dynamic and rigid fixation devices on the loads in the lumbar spine: a finite element analysis. Eur

Spine J. 2007;16: 1223–1231.

21. Massey PA, Hoge S, Nelson BG, Ogden AL, Mody MG, Myers M, Bilderback K, Solitro G, Barton RS. Nitinol Memory Rods Versus Titanium Rods: A Biomechanical Comparison of Posterior Spinal Instrumentation in a Synthetic Corpectomy Model. Global Spine J. 2021;11(3):277–282.
22. Yeung KW, Poon RW, Liu XY, Ho JP, Chung CY, Chu PK, Lu WW, Chan D, Cheung KM. Corrosion resistance, surface mechanical properties, and cytocompatibility of plasma immersion ion implantation-treated nickel-titanium shape memory alloys. J Biomed Mater Res A. 2005; 75(2): 256–267.
23. Chen CS, Shih SL.Biomechanical analysis of a new lumbar interspinous device with optimized topology. Med Biol Eng Comput. 2018;56(8):1333–1341
24. Shih SL, Chen CS, Lin HM, Huang LY, Liu CL, Huang CH, Cheng CK. Effect of spacer diameter of the Dynesys dynamic stabilization system on the biomechanics of the lumbar spine: a finite element analysis. J Spinal Disord Tech. 2012 Jul;25(5):E140-9.
25. Hahnlen, R. and M. Dapino. NiTi–Al interface strength in ultrasonic additive manufacturing composites. Composites Part B-engineering 2014;59: 101–108.

Tables

Table 1. The elements and nodes of the five finite element models.

Groups	NS/PS ratio	Node	Element
INT		94,162	112,174
Nt45	4.5/1.0	146,116	420,603
Nt35	3.5/2.0	160,660	502,535
Nt25	2.5/3.0	171,575	567,154
Nt15	1.5/4.0	191,703	688,923

PS, PCU shell; NS, nitinol stick (NS).

Table 2. Material properties of implants used in finite elements analysis.

Dynamic stabilization system		
Titanium alloy pedicle screws	Young's modulus (MPa)	110000
	Poisson's ratio	0.28
PCU shell	Young's modulus (MPa)	68.4
	Poisson's ratio	0.4
	Yield strength (MPa)	34.2
	Area (mm^2)	101.13
Nitinol stick	Young's modulus (MPa)	47000
	Poisson's ratio	0.3

Table 3. Comparison of intervertebral range of motion (degree) in finite element models

Model	Level	Flexion	Extension	Torsion	Lateral bending
INT	L2-L3	5.71	3.17	4.08	6.12
	L3-L4	5.71	2.85	4.60	6.17
Nt45	L2-L3	6.81	3.65	4.28	7.15
	L3-L4	2.28	1.09	3.79	2.63
Nt35	L2-L3	6.81	3.65	4.24	7.15
	L3-L4	2.31	1.12	4.01	2.77
Nt25	L2-L3	6.81	3.65	4.16	7.14
	L3-L4	2.38	1.18	4.22	2.96
Nt15	L2-L3	6.72	3.60	4.12	7.01
	L3-L4	2.47	1.24	4.40	3.16

Table 4. Comparison of stress of intervertebral disc (KPa) in finite element models.

Model	Level	Flexion	Extension	Torsion	Lateral bending
INT	L2-L3	893	488	678	1160
	L3-L4	810	414	751	1130
Nt45	L2-L3	1130	556	722	1440
	L3-L4	543	236	611	512
Nt35	L2-L3	1130	556	722	1430
	L3-L4	547	236	611	544
Nt25	L2-L3	1110	556	687	1430
	L3-L4	548	239	696	585
Nt15	L2-L3	1110	548	675	1400
	L3-L4	559	240	731	621

Table 5. Comparison of facet joint contact forces (N) in finite element models.

Model	Level	Flexion		Extension		Torsion		Lateral bending	
		Left	Right	Left	Right	Left	Right	Left	Right
INT	L2-L3	0	0	94	94	0	336	53	31
	L3-L4	0	0	105	105	0	336	41	9
Nt45	L2-L3	0	0	117	117	0	374	82	38
	L3-L4	0	0	6	5	0	213	0	0
Nt35	L2-L3	0	0	118	118	0	366	82	37
	L3-L4	0	0	7	7	0	245	0	0
Nt25	L2-L3	0	0	118	118	0	351	80	35
	L3-L4	0	0	11	11	0	285	1	0
Nt15	L2-L3	0	0	115	115	0	343	74	33
	L3-L4	0	0	14	15	0	323	9	0

Table 6. Comparison of the maximum stress on implants (MPa) in finite element models.

Implant	Motion	Nt45	Nt35	Nt25	Nt15
Screw	Flexion	139	140	134	130
	Extension	105	110	112	110
	Torsion	211	162	107	98.9
	Lateral bending	158	178	181	175
PCU shell	Flexion	4.7	3	3.5	4.9
	Extension	5.1	2.7	3.1	4.9
	Torsion	17.4	7.6	6	4.6
	Lateral bending	6.8	5.1	5	7.2
Nitinol stick	Flexion	44	54.6	72.4	118
	Extension	39.5	46	58.4	101
	Torsion	219	324	383	381
	Lateral bending	127	145	187	275

Figures

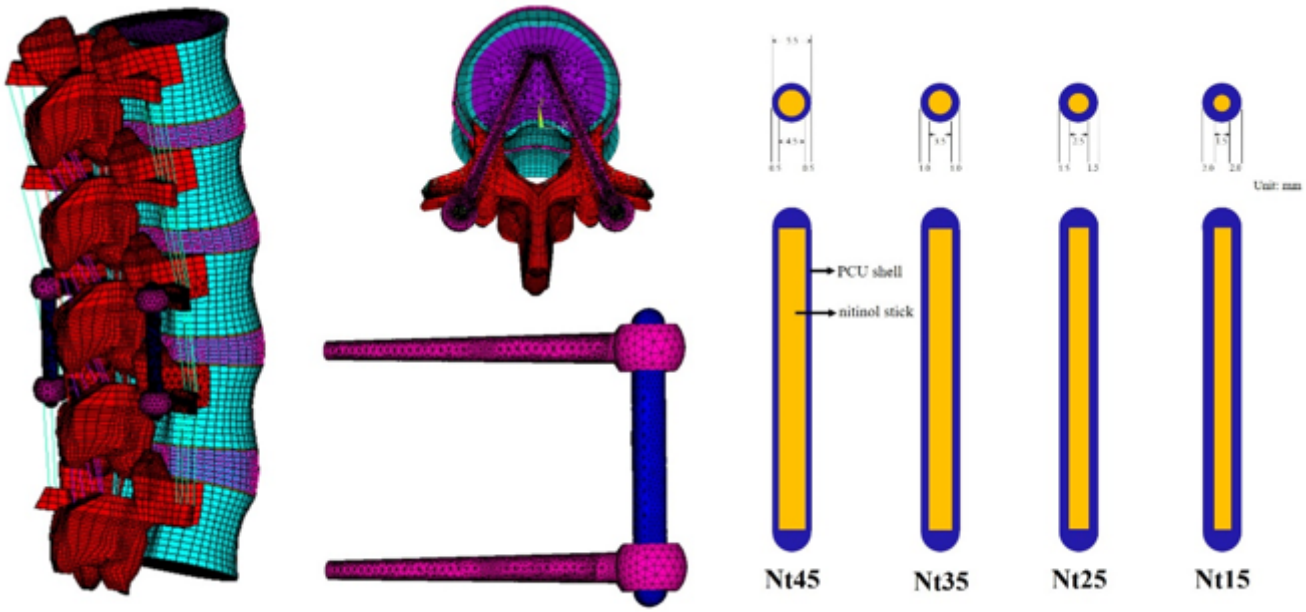

Figure 1

Overview of the finite element model and SHE rod dynamic stabilization system. Systems with different NS diameter/PS thickness ratios of the SHE rods were implanted into the L3-L4 spine model.

SHE, spinal hybrid elastic; NS, nitinol stick; PS, PCU shell.

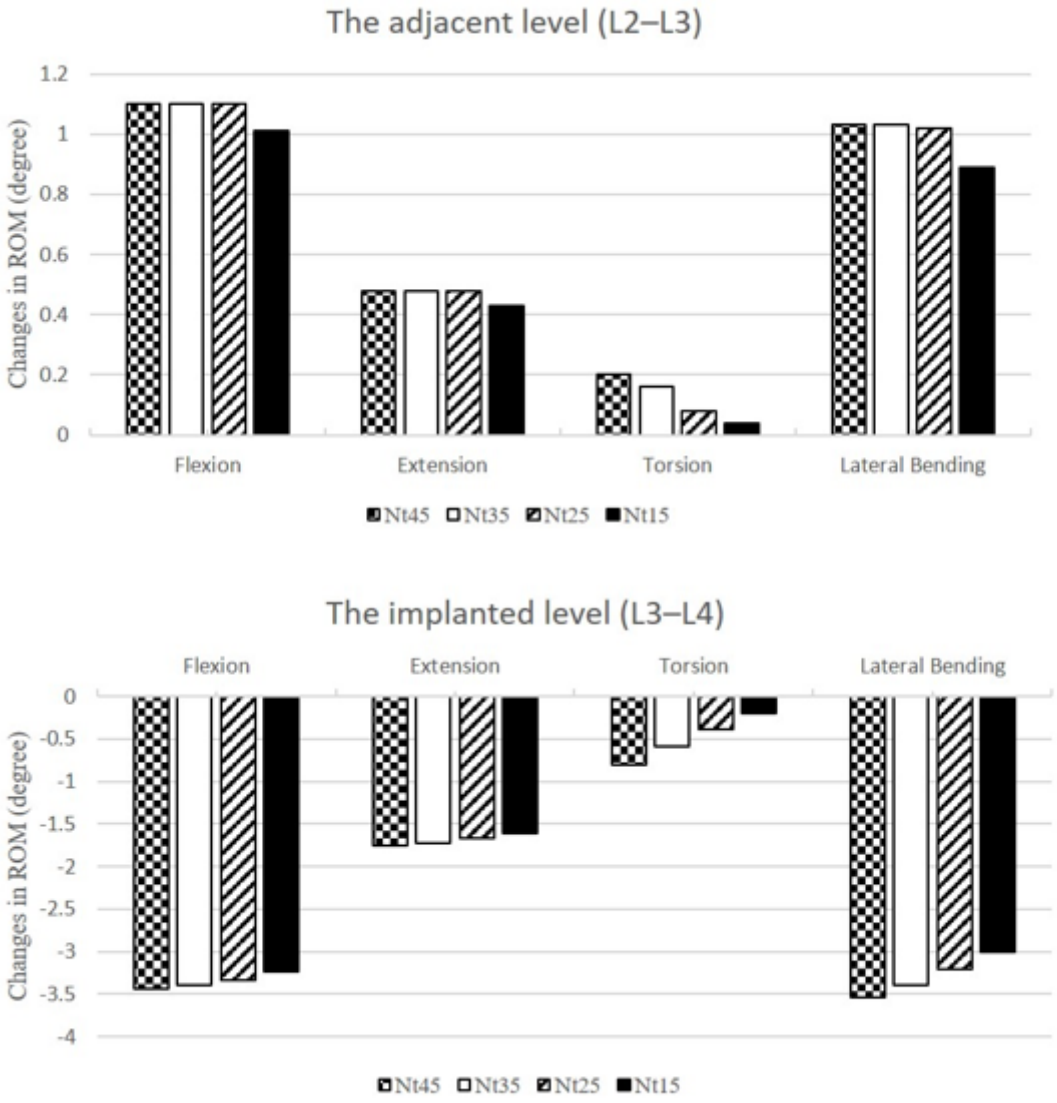

Figure 2

Changes in the ROM compared to the INT at the adjacent L2/L3 level (top) and the implanted L3/L4 level (bottom). Values for the INT are not presented because the data were normalized to the INT. The differences between these models were small. There was a downward trend in ROM changes at all levels as the NS diameter became smaller.

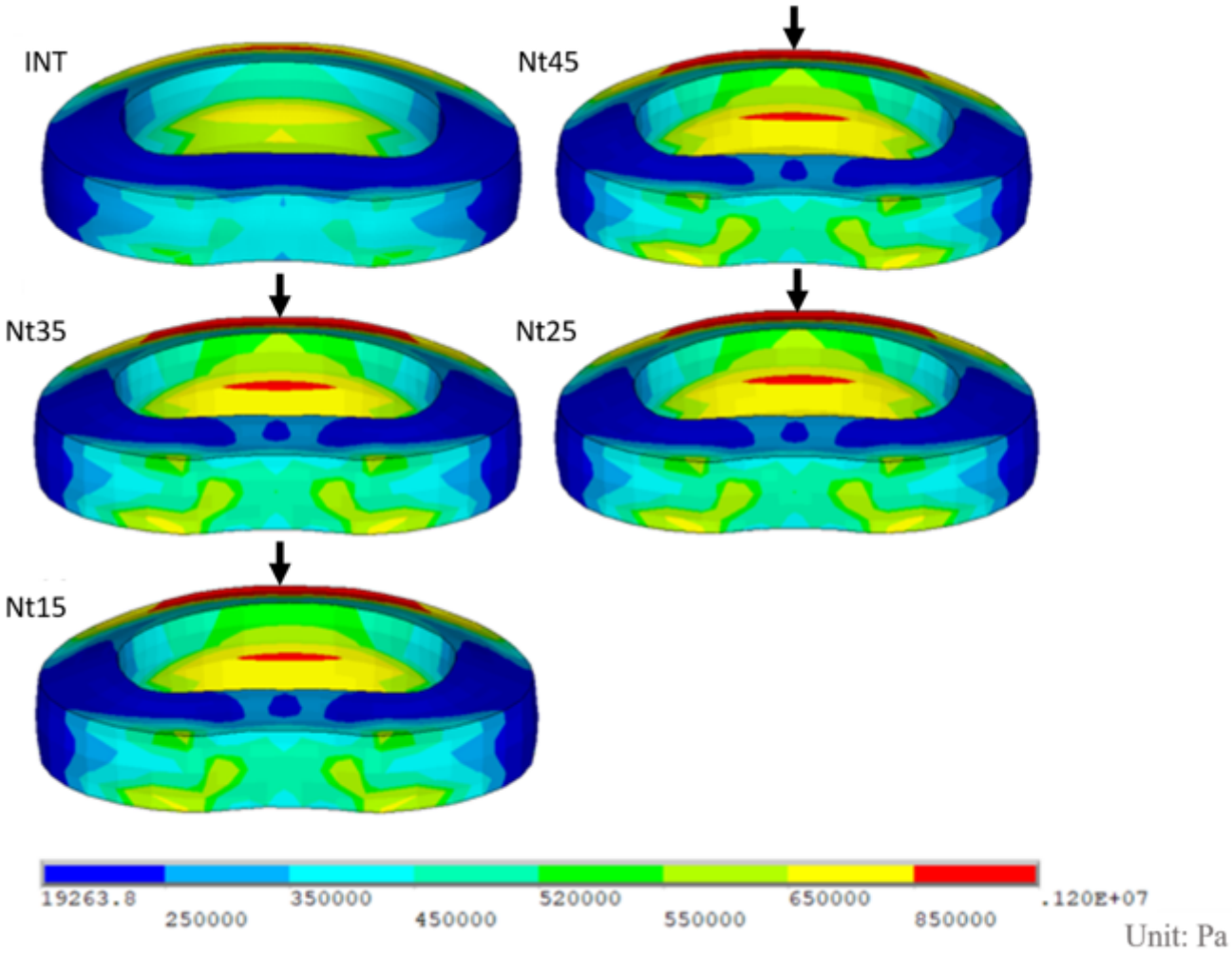

Figure 3

The von-Mises stress distribution of the adjacent L2–L3 disc in flexion. The arrow indicates the maximum at the anterior superior edge. There was no obvious trend in disc stress at the adjacent level as the NS diameter changed.

NS, nitinol stick (NS).

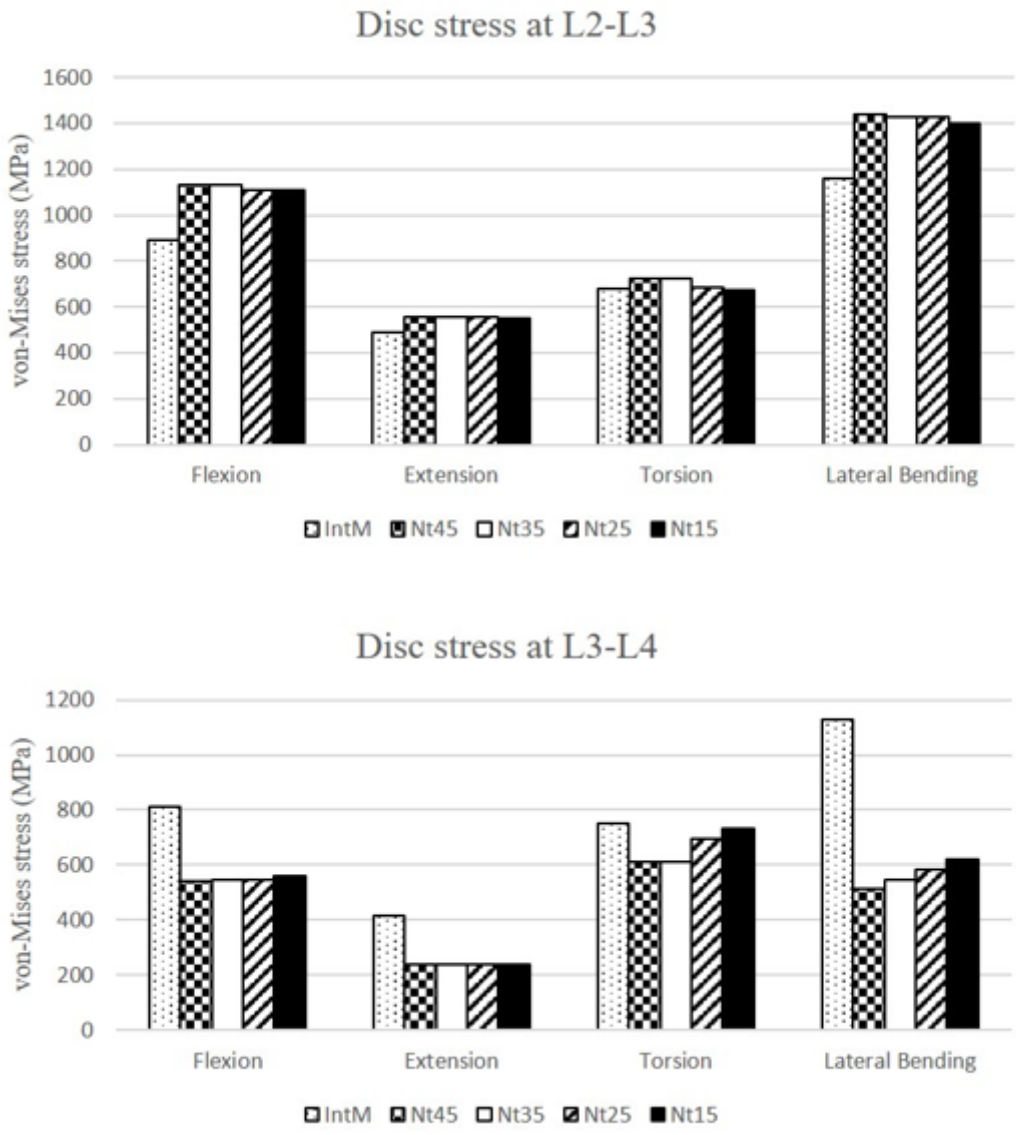

Figure 4

The von-Mises stress on the intervertebral disc. The NS diameter was inversely proportional to the disc stress at the implanted level. It did not markedly influence the disc stress at the adjacent level.

NS, nitinol stick (NS).

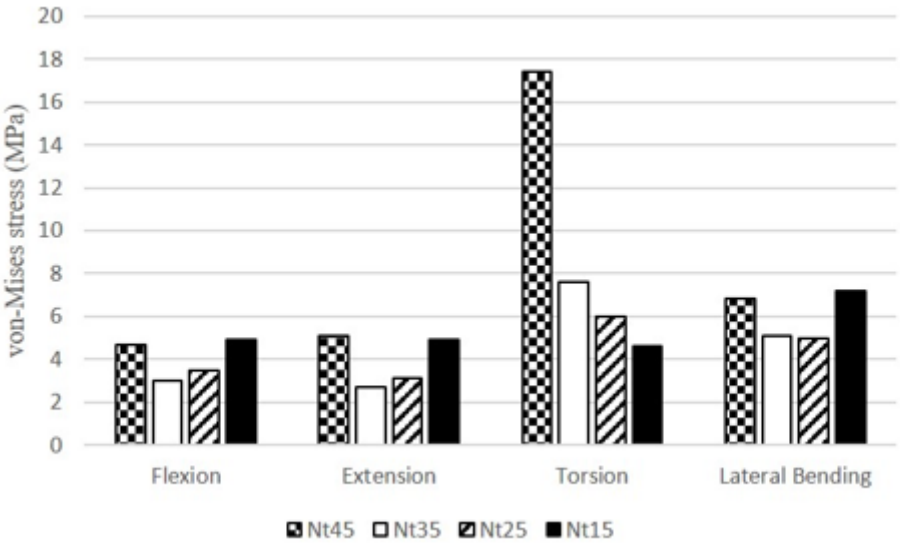

Figure 5

The von-Mises stress on the outer PS. There was no obvious trend in PS stress as the NS diameter changed.

PS, PCU shell; NS, nitinol stick.

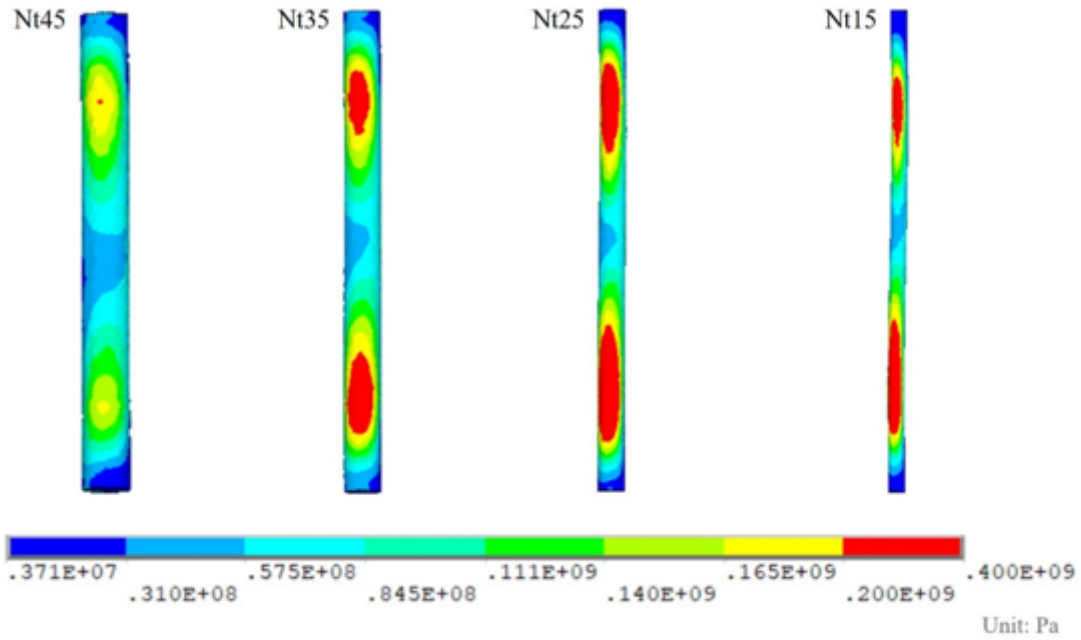

Figure 6

The von-Mises stress on the inner nitinol stick markedly increased on the upper and lower portion. The maximum occurred on the Nt25 in torsion.

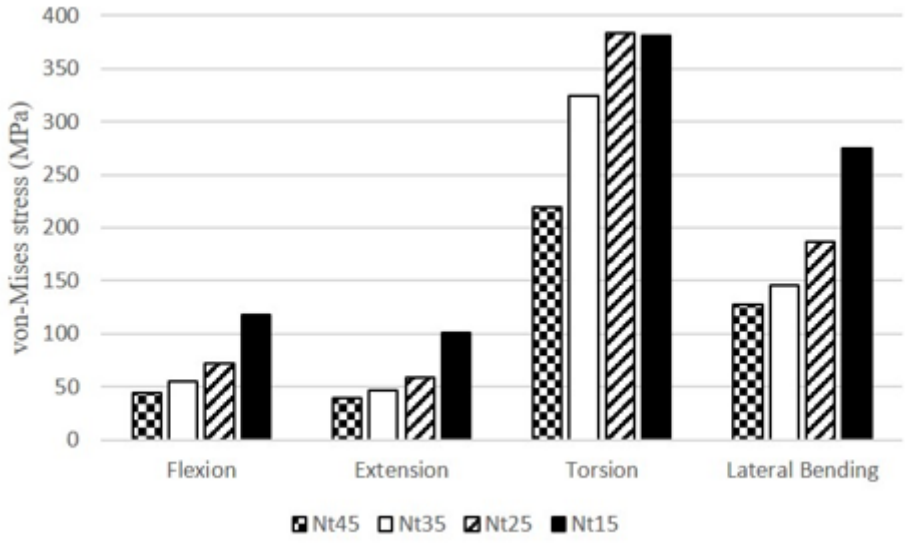

Figure 7

The von-Mises stress on the inner nitinol stick increased as the NS diameter decreased.

NS, nitinol stick (NS).

Supplementary Files

This is a list of supplementary files associated with this preprint. Click to download.

- Supp.Sherod1110407.docx